Research article

The impact of contrast retention on thrombus formation risks in patients with atrial fibrillation: A numerical study

Lan Ge [a,b,1], Yawei Xu [c,1], Jun Li [a,b,1], Yuan Li [c], Yifeng Xi [c], Xinyan Wang [a,b], Jing Wang [b], Yang Mu [b], Hongsen Wang [a,b], Xu Lu [b], Jun Guo [a,b], Zengsheng Chen [c], Tao Chen [a,b,*], Yundai Chen [a,b,**]

[a] Medical School of Chinese PLA, 28 Fuxing Road, Haidian District, Beijing 100853, China
[b] Senior Department of Cardiology, the Sixth Medical Center of PLA General Hospital, 6 Fucheng Road, Haidian District, Beijing 100048, China
[c] Key Laboratory of Biomechanics and Mechanobiology (Beihang University), Ministry of Education, Beijing Advanced Innovation Center for Biomedical Engineering, School of Biological Science and Medical Engineering, Beihang University, Beijing, 100083, China

ARTICLE INFO

ABSTRACT

Background: Contrast retention (CR) is an important predictor of left atrial appendage thrombus (LAAT) and stroke in patients with non-valvular atrial fibrillation (AF). We sought to explore the underlying mechanisms of CR using computational fluid dynamic (CFD) simulations.

Methods: A total of 12 patients with AF who underwent both cardiac computed tomography angiography (CTA) and transesophageal echocardiography (TEE) before left atrial appendage occlusion (LAAO) were included in the study. The patients were allocated into the CR group or non-CR group based on left atrial appendage (LAA) angiography. Patient-specific models were reconstructed to evaluate time-averaged wall shear stress (TAWSS), oscillatory shear index (OSI), relative residence time (RRT), and endothelial cell activation potential (ECAP). Additionally, the incidence of thrombosis was predicted using residence time (RT) at different time-points.

Results: TAWSS was lower [median (Interquartile Range) 0.27 (0.19–0.47) vs 1.35 (0.92–1.79), $p < 0.001$] in LAA compared to left atrium. In contrast, RRT [1438 (409.70–13869) vs 2.23 (1.81–3.14), $p < 0.001$] and ECAP [122.70 (30.01–625.70) vs 0.19 (0.16–0.27), $p < 0.001$] was higher in the LAA. The patients in the CR group had significantly higher RRT [(mean ± SD) 16274 ± 11797 vs 639.70 ± 595.20, $p = 0.009$] and ECAP [610.80 ± 365.30 vs 54.26 ± 54.38, $p = 0.004$] in the LAA compared to the non-CR group. Additionally, patients with CR had a wider range of thrombus-prone regions [0.44(0.27–0.66)% vs 0.05(0.03–0.27)%, $p = 0.009$] at the end of the 15th cardiac cycle.

Conclusions: These findings suggest that CR might be an indicator of high-risk thrombus formation in the LAA. And CT-based CFD simulation may be a feasible substitute for the evaluation of LAA thrombotic risk in patients with AF, especially in patients with CR.

* Corresponding author. Senior Department of Cardiology, the Sixth Medical Center of PLA General Hospital, 6 Fucheng Road, Haidian District, Beijing 100048, China.
** Corresponding author. Senior Department of Cardiology, the Sixth Medical Center of PLA General Hospital, 6 Fucheng Road, Haidian District, Beijing 100048, China.
E-mail addresses: chentao301@126.com (T. Chen), cyundai@vip.163.com (Y. Chen).
[1] These authors contributed equally to this work.

Abbreviations

AF	Atrial fibrillation
CFD	Computational fluid dynamic
CR	Contrast retention
CTA	Computed tomography angiography
ECAP	Endothelial cell activation potential
LA	left atrium
LAA	Left atrial appendage
LAAO	Left atrial appendage occlusion
LAAT	Left atrial appendage thrombus
LVEF	Left ventricular ejection fraction
OSI	Oscillatory shear index
PV	Pulmonary vein
RRT	Relative residence time
RT	Residence time
TAWSS	Time-averaged wall shear stress
TEE	Transesophageal echocardiography

---

1. Introduction

Atrial fibrillation (AF) is one of the most prevalent arrhythmias globally, and is associated with a 5-fold increased risk of stroke [1, 2]. Majority of the thromboembolic events in nonvalvular AF are caused by thrombi originating in the left atrial appendage (LAA) [3, 4]. Left atrial appendage occlusion (LAAO) has emerged as a non-pharmacological stroke prevention strategy for patients with non-valvular AF who are not suitable candidates for long-term oral anticoagulation. The contrast retention (CR) phenomenon is defined as a visible contrast media residue within the LAA that persists more than 15 heartbeats after the LAA angiography during the LAAO procedure. There is a significant positive correlation between CR in LAA angiography, left atrial appendage thrombus (LAAT), and stroke [5,6]. This indicates that CR is a potential predictor for LAAT and stroke. However, the underlying mechanisms of this CR phenomenon are incompletely understood.

Computational fluid dynamics (CFD), which is a subfield of fluid mechanics, can now provide sufficient hemodynamic information for the quantitative detection of cardiovascular hemodynamics. With the advancement of CFD simulation, we can now understand the hemodynamic characteristics of left atrium (LA) and LAA, the impact of AF on LA/LAA hemodynamics, and the underlying hemo-dynamics associated with LA thrombosis [7,8,9,10,11,12,13,14]. While certain physiological models may reflect the hemodynamic alterations brought about by atrial fibrillation, the accuracy of CFD simulation results is reduced due to the high heterogeneity of LAA, which can cause simulation results unique to a few populations to diverge from the population as a whole [15,16,17,18].

In this study, we generated individual CFD models to investigate the hemodynamics in patients with AF. Additionally, we explored the underlying hemodynamic mechanisms of the CR phenomenon.

2. Methods

2.1. Study population and groups

This single-center, retrospective study included all patients who underwent percutaneous left atrial appendage occlusion (LAAO) procedures from November 2021 to February 2023 at the Sixth Medical Centre of the Chinese PLA General Hospital. The inclusion criteria were as follows: (1) aged 18–85 years; (2) non-valvular AF; (3) LAAO; and (4) transesophageal echocardiography (TEE) (including pulmonary vein (PV) flows and LAA velocity analysis) and cardiac CT (including the full atrium and pulmonary vein anatomy) performed before the LAAO procedure was conducted. The exclusion criteria were as follows: (1) structural heart disease; (2) insufficient cardiac CT imaging for LA/LAA model construction; and (3) insufficient TEE imaging. The patients were then divided into two groups based on the observation of CR phenomenon during LAA angiography: CR group (n = 6) and non-CR group (n = 6). This research protocol was approved by the appointed local ethics committee. The need for written informed consent was waived due to the retrospective nature of the study.

2.2. CT acquisitions

The CT acquisition protocol has previously been described [19]. In brief, periprocedural prospective ECG gating multidetector CT (dual-source FLASH high-pitch spiral, SIEMENS Definition) was used to reconstruct and evaluate the left atrium (LA) and the LAA. Approximately 60 ml of iopromide (Ultravist 370, Bayer Healthcare, Berlin, Germany) was injected with a double-barrelled high--pressure CT syringe at a flow rate of 4.0–5.0 mL/s through a median cubital vein.

2.3. LAA angiography and CR assessment

Under general or basic anesthesia, the femoral vein was used to provide venous access. The transseptal puncture was carried out in the inferior-posterior region of the oval foramen. The left atrial pressure was measured before the angiography. Contrast medium was then injected into the LAA using the 14F access sheath and 5F pigtail catheter simultaneously in the right anterior oblique (RAO) 30° and caudal (CAU) 20°. Within 3 s, 15 ml of contrast medium was administered through the pigtail catheter at a slow to fast injection rate, followed by a long cine angiography lasting at least 15 consecutive cardiac cycles to examine the contrast agent filling and clearance in the LAA. The patient was divided into two groups based on whether the contrast was still seen in the LAA after 15 cardiac cycles: CR group and non-CR group. The morphological types and the lobes of LAA were measured.

2.4. Image Segmentation

The patient-specific LA/LAA geometry was generated using Mimics Medical 17.0 (Materialise, Belgium) using the CT scans at 30–40% of the RR interval. The PVs, LA and LAA walls, and the plane of the mitral valves (excluding valves) were all included in the extracted surface. Then, extracted surfaces were smoothed out by removing spikes and reducing noise using Geomagic Studio (Geo-Magic Inc, USA), and all the inlet and outlet geometric boundaries were cropped to generate a flat surface [20]. Next, the SOLID-WORKS software was used to lengthen the entry lengths to lessen the entrance effects [21]. To minimize the impact of mitral valve discrepancies on atrial hemodynamics, all patients were given an identical mitral valve area (mitral valve diameter 13 mm) to exclude substantial mitral regurgitation. Tetrahedral elements were used for volumetric meshing in the LA and LAA volume by using five wall prism layers using the ANSYS Workbench 2021R1 (ANSYS, USA). The base element size was set at 1 mm, and the mesh entity with a maximum element size of 0.5 mm was created in the LAA region for the localized complex geometric structures, yielding 6–10 million elements for each patient depending on the size of the LA. The size of mesh components was thus modified to appropriately reflect topology based on surface curvature [13]. Various mesh sizes were produced for meshing convergence investigation, and the final meshes provided were optimal and did not compromise solution accuracy. A schematic depiction of the workflow designed and developed in this study is shown in Fig. 1.

2.5. Boundary conditions

The patient-specific PV flow profiles were extracted from the TEE data to obtain the final velocity profile by digitizing and generating points on the waves. We use only one patient-specific PV velocity Doppler profile as the inlet boundary condition of all 4/5
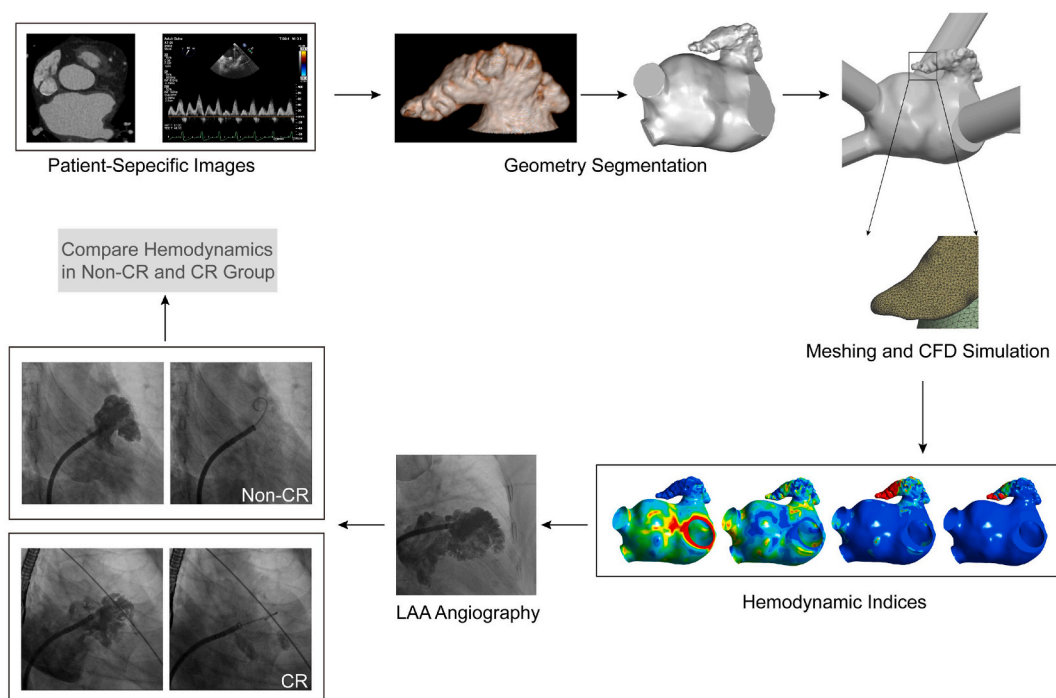

Fig. 1. A schematic depiction of the workflow designed and developed in this study. Firstly: patient-specific data processed to derive individualized LA/LAA anatomical CFD models. Secondly: personalized boundary conditions are applied for CFD simulation, and the simulation results were post-processed to derive hemodynamics indices. Thirdly: comparison of hemodynamic indices between the CR and non-CR groups based on the LAA angiography results. Abbreviations: CFD, computational fluid dynamics; CR, contrast retention.

PV in this simulation because not all of the 4/5 PV velocity Doppler profiles are available for every case, and prior research has shown that cases where the velocities are all four left PVs or all four right PVs do not differ much from the case with four different PVs [15]. The mitral valve was under zero pressure throughout the simulation to reduce computational expenses. Given that atrial flow has been found to have a Reynolds number of less than 2 300, it was presumed that the blood flow was in the laminar regime.

2.6. Computational fluid dynamics simulation

Ansys CFX 2021R1 (ANSYS, USA) was used for the simulation. Blood was defined as an incompressible, Newtonian fluid with a constant density and viscosity of 1050 kg/m^3 and 0.0035 Pa s, respectively. The LA and LAA walls were assumed to be rigid and non-slip. The calculations were run with a time step of 0.01 s and 100 iterations per time step to ensure solution convergence. Residuals of mass and momentum conservation equations <0.001 were considered absolute convergence criteria. We simultaneously set up massflow monitoring during the computation, and when the entire inlet massflow equals the outlet massflow, we consider the calculation to have converged. Five transient simulations were carried out to guarantee stability and mitigate the effects of transition. The flow was totally periodic after the third cycle, and no significant differences were found. The last cardiac cycle was used for all the analyses.

2.7. Hemodynamic indicators

The CFD simulation results were further processed using CFD-Post 2021R1 (ANSYS, USA). The most important hemodynamic characteristics, which are derived from wall shear stress and used to explain LAA fluid dynamics and related thrombus formation, including time-averaged wall shear stress (TAWSS), oscillatory shear index (OSI), relative residence time (RRT), and endothelial cell activation potential (ECAP) were computed using MATLAB R2021b (The Mathworks, USA) [22,23,24]. The definitions of these four indices are given in Equations (1)–(4), respectively.

$$TAWSS = \frac{1}{t}\int_0^T |WSS|dt \tag{1}$$

$$OSI = 0.5 \times \left[1 - \frac{\left|\int_0^T WSSdt\right|}{\int_0^T |WSS|dt}\right] \tag{2}$$

$$RRT = \frac{1}{[(1 - 2 \times OSI) \times TAWSS]} \tag{3}$$

$$ECAP = \frac{OSI}{TAWSS} \tag{4}$$

2.8. Residence time and thrombosis-prone region

The extra variable RT (residence time) was applied to identify the time blood stays in various fluid regions and obtain qualitative information on areas that are more susceptible to blood stagnation. This was modeled as a passive tracer conveyed with flow and simulated as done in previous studies [25,24]. RT was solved using the transport equation provided below:

$$\frac{\partial RT}{\partial t} + v \times \nabla RT = D_{RT}\nabla^2 RT + 1$$

v = Blood flow speed;
t = Time;
D_{RT} = blood self-diffusion rate ($D_{RT} = 1.14 \times 10{-}11$ m^2 s^{-1}).
The initial value of RT was set to 0, and the source term "1″ refers to a unit increase in RT for each unit increase in time.
Given that the RT value represents the time it takes for blood to enter and stay in the LA and LAA, we use it as a reference to calculate the regions that have a RT value greater than 5th/10th/15th cardiac cycle, which represent the areas in the LA and LAA that are least prone to blood exchange, and refer to this area as the thrombosis-prone region.

2.9. Statistics

The statistical analysis was conducted using GraphPad Prism 9 (GraphPad Software, USA) and SPSS (SPSS 26, SPSS Inc., USA). The Shapiro–Wilk test was used to assess normality of data distribution. Continuous variables that conformed to normal distribution were described as mean ± standard deviation. Data with skewed distribution are described as median (interquartile range). The student's t-

test was used to compare the means for data with normal distribution; otherwise, the Mann-Whitney test was used. The paired *t*-test or Wilcoxon signed-rank test was used to compare paired data depending on data distribution. Categorical variables were summarized as frequency (percentage) and compared using Pearson's chi-square test (or Fisher's exact test whenever needed). A two-tailed P value < 0.05 was considered statistically significant.

3. Results

3.1. Demographics and morphological characteristics

After reviewing medical records of patients admitted to our center from November 2021 to February 2023, a total of 48 patients were identified on initial screening for the LAAO cohort. Of the 48 patients, 33 were excluded for lacking velocity profiles at the PV, and 3 were excluded because the left atrium was not completely covered by cardiac CT. Finally, 12 patients were enrolled in this study. Patient characteristics are summarized in Table 1. There were no significant (p > 0.05) differences between the two groups with regards to age, gender, CHA$_2$DS$_2$-VASc score, AF type, hypertension, heart failure, vascular disease, cardiogenic stroke or systemic embolism, diabetes, and left ventricular ejection fraction (LVEF). Morphological parameters of the LA/LAA are also presented in Table 1. Additionally, there were no significant variations in LA volume, LAA volume, LAA depth, LA anteroposterior diameter, the number of lobes, or LAA morphology between the two groups.

3.2. Comparison of hemodynamic parameters in the LA and LAA

Hemodynamic parameters in the LA and LAA are compared among all patients. Notably, the TAWSS values were quantitatively and significantly lower in the LAA compared to the LA [0.27(0.19–0.47) vs 1.35 (0.92–1.79), p < 0.001] (Fig. 2a). Additionally, there were significantly higher RRT [1438(409.70–13869) vs 2.23(1.81–3.14), p < 0.001] and ECAP [122.70(30.01–625.70) vs 0.19 (0.16–0.27), p < 0.001] values in the LAA compare to other parts of the LA (Fig. 2b). The distributions of OSI in the LA and LAA were similar (Fig. 2a).

3.3. Comparison of hemodynamic parameters in the CR and Non-CR group

Average hemodynamics comparison showed that both the RRT and ECAP values of the LAA were significantly higher in CR group compared to the non-CR group [p = 0.009 and p = 0.004 for RRT and ECAP, respectively] (Fig. 2c and d). However, the differences between LAA TAWSS and OSI between the two groups were not statistically significant (p = 0.10 and 0.52, respectively) (Figs. S1 and S2). There were no significant differences in the LA hemodynamics between the two groups. The distribution of RRT and ECAP magnitude over the LA/LAA is illustrated in Fig. 3.

3.4. Thrombosis prediction using RT

There was no statistical difference in the proportion of thrombus-prone areas between the CR and non-CR groups at the time of the 5th cardiac cycle [2.22 ± 0.93% vs. 1.01 ± 1.02%; p = 0.06]. At the time of the 10th cardiac cycle, the thrombus-prone region in the CR group was larger than the non-CR group [0.64 ± 0.31% vs. 0.24 ± 0.24%; p = 0.03]. At the end of the 15th cardiac cycle, all

Table 1
Demographics and morphological characteristics. Continuous variables were reported as means ± standard deviations or medians (interquartile ranges), and categorical variables were reported as n (%). Abbreviations: AF, atrial fibrillation; LA, left atrium; LAA, left atrial appendage; LVEF, left ventricular ejection fraction; CR, contrast retention; n, number; ml, milliliter; mm, millimeter.

|	Non-CR group (n = 6)	CR group (n = 6)	*P*-value
Age, year	59.8 ± 7.1	66.7 ± 4.1	0.07
Gender, male, *n* (%)	5 (83.3%)	4 (66.7%)	>0.99
CHA$_2$DS$_2$-VASc score	3.5 (3–5)	4 (2.8–5.3)	0.87
AF type			0.24
Persistent AF, *n* (%)	2 (33.3%)	5 (83.3%)	
Paroxysmal AF, *n* (%)	4 (66.7%)	1 (16.7%)	
Hypertension, *n* (%)	4 (66.7%)	2 (33.3%)	0.45
Heart failure, *n* (%)	1 (16.7%)	1 (16.7%)	>0.99
Vascular disease, *n* (%)	3 (50.0%)	3 (50.0%)	>0.99
Cardiogenic Stroke or systemic embolism, *n* (%)	2 (33.3%)	3 (50.0%)	>0.99
Diabetes, *n* (%)	2 (33.3%)	1 (16.7%)	>0.99
LVEF (%)	59.7 ± 5.1	57.8 ± 9.0	0.67
LA Volume (ml)	146.4 ± 60.8	160.3 ± 37.1	0.64
LAA Volume (ml)	10.3 ± 3.7	14.2 ± 5.8	0.20
LAA Depth (mm)	39.4 (31.8–41.9)	42.1 (40.7–46.4)	0.13
LA anteroposterior diameter (mm)	39.5(36.5–44.8)	44(40.8–48.3)	0.33
Number of Lobes	2.5(1.8–3.3)	3(2–3)	0.87
LAA Morphology (Chicken Wing)	2(33.3%)	0(100%)	0.45
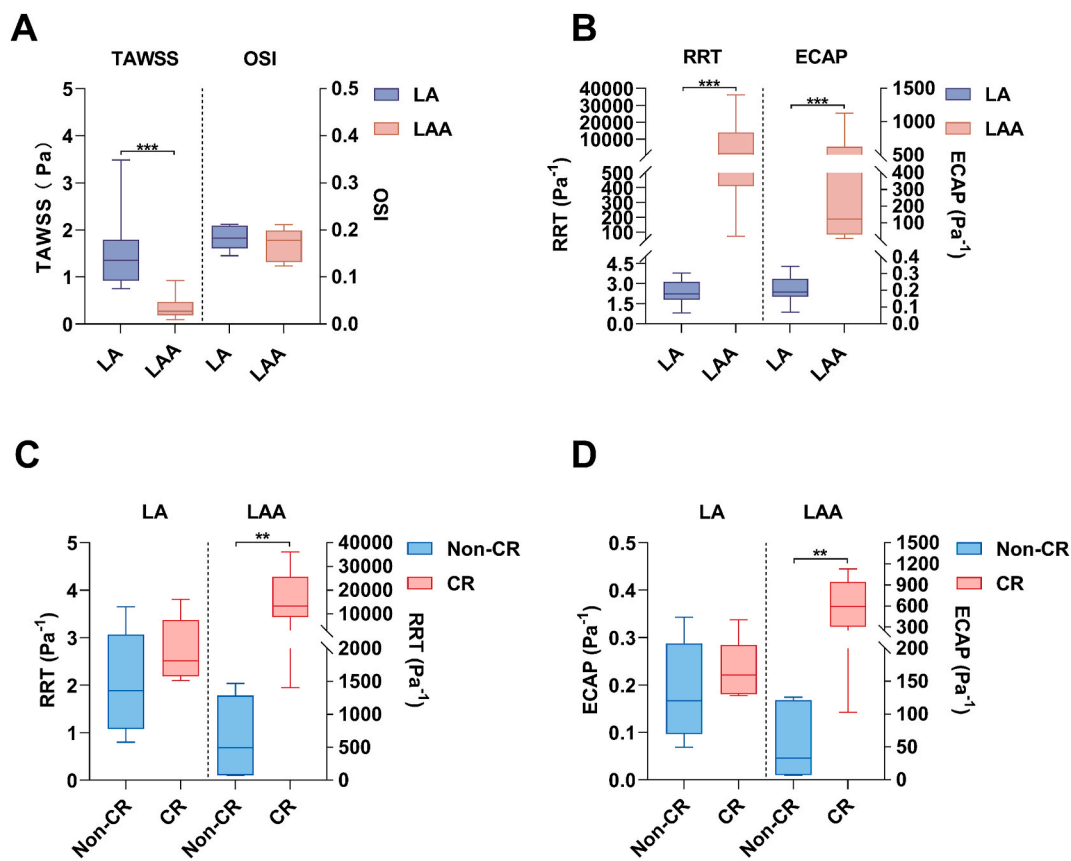
Fig. 2. Hemodynamic parameters comparison between LA and LAA (a, b); Hemodynamic parameters comparison between CR group and non-CR group in LA/LAA (c, d). Abbreviations: LA, left atrial; LAA, left atrial appendage; CR, contrast retention; TAWSS, time averaged wall shear stress; OSI, oscillatory shear index, RRT, the relative residence time; ECAP, the endothelial cell activation potential.

thrombus was located at the tip of the LAA, and the CR group considerably widened the scope of thrombus-prone regions. The median normalized volume of residual passive tracer in the non-CR group was 0.05(0.03–0.27) %, compared to 0.44(0.27–0.66) % in the CR group(p = 0.009). Fig. 4 depicts the formation of the thrombus predicted by RT at the 15th cardiac cycle.

4. Discussion

This study analyzed personalized CFD simulations to compare the hemodynamic parameters of LA/LAA and explored the mechanism of the CR phenomenon. The major findings of the present study are as follows: (1) LAA in patients with AF had lower TAWSS and higher RRT and ECAP compared to the LA, suggesting that the LAA is more thrombogenic than the LA; (2) Patients with CR had a higher RRT and ECAP in the LAA, indicating a prothrombotic milieu compared to non-CR patients; and (3) Patients with CR had more stagnant flow in the LAA, suggesting the patients with CR have a wider thrombus-prone region.

TAWSS and OSI are the most commonly employed indices for the diagnosis of endothelial damage zones using CFD simulations in patients with AF [8,17,24]. RRT combines TAWSS and OSI to represent the time blood spends near the wall [20]. The ECAP is based on the ratio of OSI to TAWSS and highlights regions of aberrant hemodynamics in vascular flow and higher endothelial susceptibility, making it a more reliable index for assessing the risk of thrombus formation [26]. Our CFD simulations demonstrated that the TAWSS value of the LAA is significantly lower than the LA. These results align with the findings of previous CFD investigations [17,27,24]. Notably, RRT and ECAP in the LAA were considerably greater in all patients compared to the LA. This suggests that RRT and ECAP are more sensitive detectors of abnormal hemodynamic zones, which is consistent with Wu et al.'s findings [28]. Prior research has indicated that certain patients with AF have high OSI values in the LAA, while others also have high OSI values in the atrium, indicating the heterogenicity of OSI [24]. There were no significant variations in OSI distributions between the LA and LAA, which was likely due to the small sample size. Further studies are thus required to validate these findings. These findings, based on CFD, can explain why thrombi primarily formed in the LAA of patients with AF. Additionally, this clarifies the primary formation of CR in the LAA as opposed to the LA.

Previous research indicated that the CR phenomenon was an independent risk factor for LAAT [6]. A recent cross-sectional study also found that CR was independently related to stroke in patients with AF, and that the combination of CR can enhance the
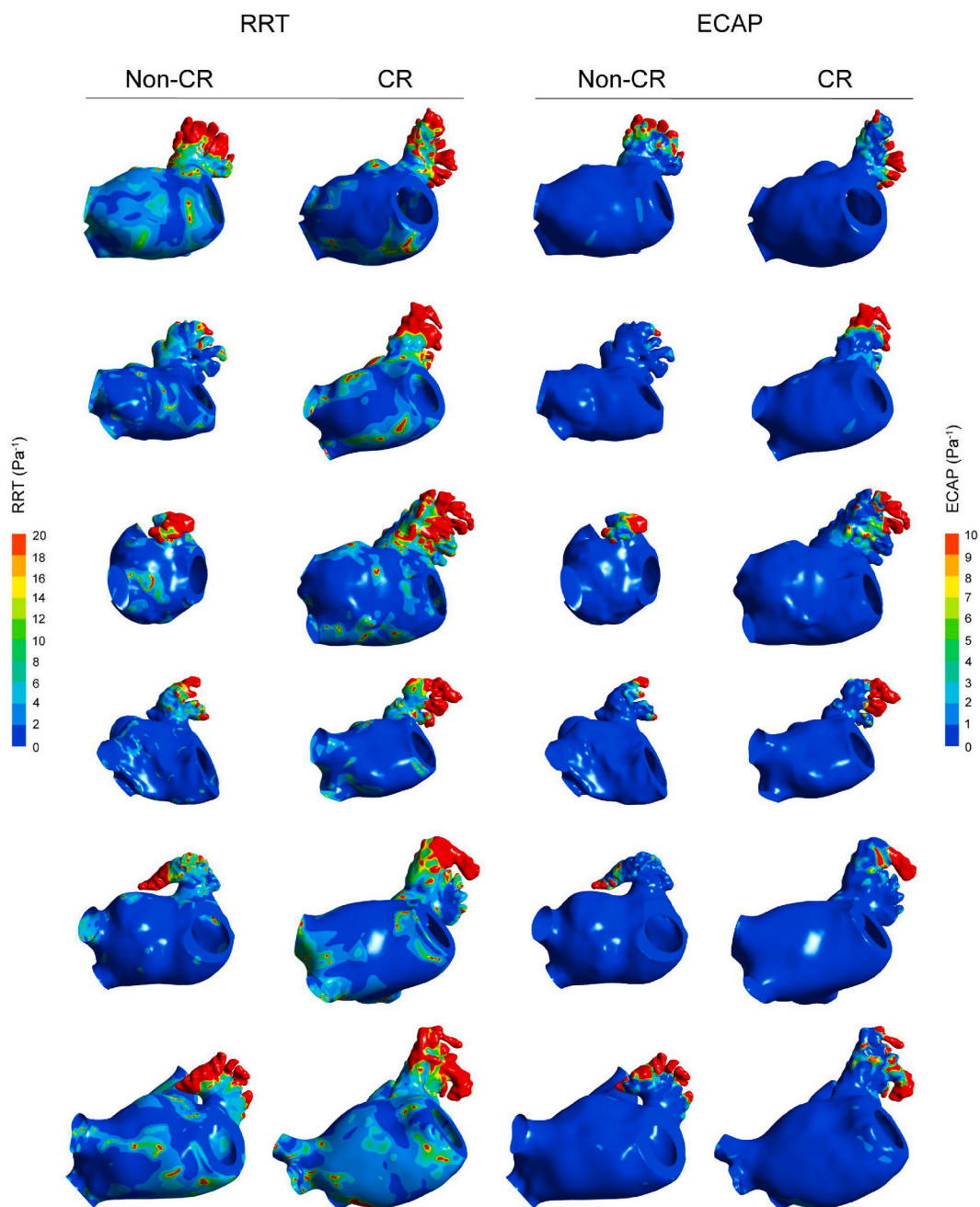
Fig. 3. Patients' distribution of RRT and ECAP contours of the LA/LAA. Abbreviations: LA, left atrial; LAA, left atrial appendage; CR, contrast retention; RRT, the relative residence time; ECAP, the endothelial cell activation potential.

CHA_2DS_2-VASc stratification system for stroke risk prediction [5]. There was no significant difference in any of the hemodynamic indicators in the LA when comparing the CR and non-CR groups. However, the LAA of the CR group showed significantly higher RRT and ECAP values compared to the non-CR group. This suggests that the CR phenomenon was predominantly produced by local hemodynamic alterations in the LAA and that the CR group was at a higher risk of thrombosis. These outcomes support the findings of our previous retrospective study [6].

In the present investigation, blood flow through the LA was timed using the passive scalar technique and the thrombus-prone regions in the LA were predicted based on the RT value at different time-point. There were no significant differences in the proportion of thrombus-prone areas between the CR and non-CR groups by the 5th cardiac cycles. However, the CR group had a significantly wider range of thrombus prone areas at the 10th or 15th cardiac cycles. This indicates that the CR group has reduced temporal efficiency of LAA emptying. The CFD-derived RT simulation was consistent with CR clinical observations; however, more data is
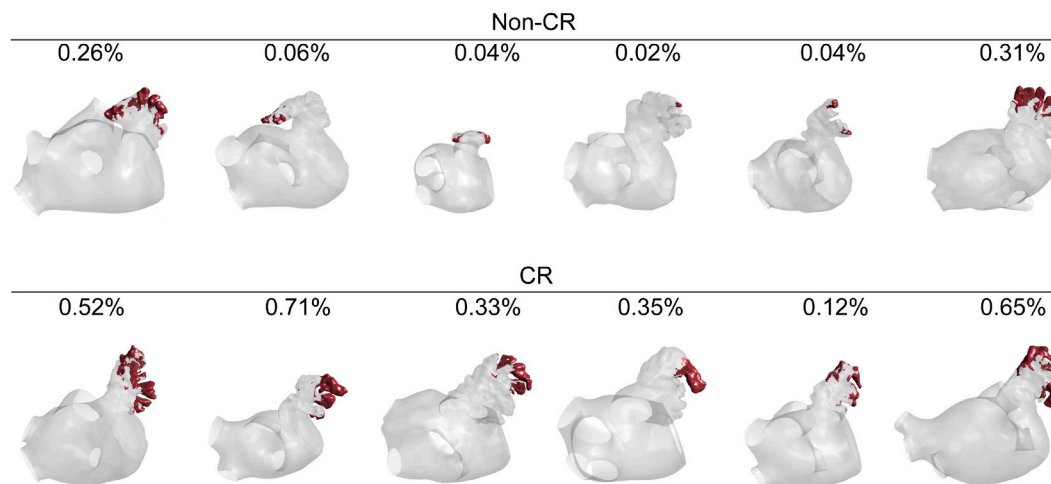
Fig. 4. The distributions and thrombus volume proportions predicted by RT between CR group and non-CR group at the 15th cardiac cycle. Red indicates the thrombus-prone area. Abbreviations: CR, contrast retention.

required to further define its role in LAA thrombus-prone area prediction and to assist in future LAAO location optimization. Additionally, we found that the predicted thrombus-prone areas were mostly located at the tip and body of the LAA, especially the distal lobes of LAA. Our findings align with those of Luis Marroquin et al., who reported on 126 patients with LAA thrombi, which included 63.9% and 18.5% thrombi localized at the tip and body of the LAA, respectively [29].

The present study had some limitations. Firstly, despite the patient's unique mitral valve morphology and movement, which may have an impact on the LAA dynamics, our CFD simulation was implemented with constant parameters to minimize variations during the calculation process. Secondly, although our study's sample size is considerable, a larger sample size in a follow-up study would enable a more precise evaluation of LA/LAA hemodynamics utilizing MDCTA. Thirdly, the mitral valve was assumed to be open throughout the simulation as an outlet boundary condition, which is inconsistent with real conditions. Therefore, more complex numerical approaches and more accurate boundary conditions may produce more realistic simulations in the future.

5. Conclusion

This study employed CFD models to investigate the mechanism CR phenomenon. We used patient-specific boundary conditions and geometries to numerically simulate LA/LAA hemodynamics in patients with or without CR, and computed a number of reliable indicators that had been used previously. Our results identified significant potential indicators for the identification of LAA with a high risk of stroke. This will assist clinicians in the selection of individualized therapies, thus improving clinical prognosis.

Funding

CRediT authorship contribution statement

Lan Ge: Conceptualization, Data curation, Formal analysis, Methodology, Software, Visualization, Writing – original draft, Writing – review & editing. **Yawei Xu:** Formal analysis, Methodology, Visualization, Writing – review & editing. **Jun Li:** Data curation, Formal analysis, Methodology, Visualization, Writing – review & editing. **Yuan Li:** Methodology, Visualization, Writing – review & editing. **Yifeng Xi:** Methodology, Visualization, Writing – review & editing. **Xinyan Wang:** Data curation, Methodology, Writing – review & editing. **Jing Wang:** Data curation, Methodology, Writing – review & editing. **Yang Mu:** Data curation, Methodology, Writing – review & editing. **Hongsen Wang:** Methodology, Software, Writing – review & editing. **Xu Lu:** Formal analysis, Methodology, Software, Writing – review & editing. **Jun Guo:** Conceptualization, Funding acquisition, Writing – review & editing. **Zengsheng Chen:** Conceptualization, Methodology, Visualization, Writing – review & editing. **Tao Chen:** Conceptualization, Methodology, Supervision, Writing – review & editing. **Yundai Chen:** Supervision, Writing – review & editing, Conceptualization.

Declaration of competing interest

The authors declare that they have no known competing financial interests or personal relationships that could have appeared to influence the work reported in this paper.

Acknowledgments

Appendix A. Supplementary data

Supplementary data to this article can be found online at https://doi.org/10.1016/j.heliyon.2024.e26792.

References

[1] J. Kornej, C.S. Borschel, E.J. Benjamin, R.B. Schnabel, Epidemiology of atrial fibrillation in the 21st Century: Novel methods and new Insights, Circ. Res. 127 (1) (2020) 4–20.

[2] T.J. Wang, J.M. Massaro, D. Levy, R.S. Vasan, P.A. Wolf, R.B. D'Agostino, et al., A risk score for predicting stroke or death in individuals with new-onset atrial fibrillation in the community: the Framingham Heart Study, JAMA 290 (8) (2003) 1049–1056.

[3] N.M. Al-Saady, O.A. Obel, A.J. Camm, Left atrial appendage: structure, function, and role in thromboembolism, Heart 82 (5) (1999) 547–554.

[4] R. Beigel, N.C. Wunderlich, S.Y. Ho, R. Arsanjani, R.J. Siegel, The left atrial appendage: anatomy, function, and noninvasive evaluation, JACC Cardiovasc Imaging 7 (12) (2014) 1251–1265.

[5] L. Jiang, Z. Hao, X. Xie, K. Xu, L. Shen, X. Pan, et al., Left atrial appendage angiography for stroke risk prediction in patients with atrial fibrillation, EuroIntervention (2023).

[6] X. Lu, T. Chen, G. Liu, Y. Guo, X. Shi, Y. Chen, et al., Relations between left atrial appendage contrast retention and thromboembolic risk in patients with atrial fibrillation, J. Thromb. Thrombolysis 53 (1) (2022) 191–201.

[7] G.M. Bosi, A. Cook, R. Rai, L.J. Menezes, S. Schievano, R. Torii, et al., Computational fluid dynamic analysis of the left atrial appendage to Predict thrombosis risk, Front Cardiovasc Med 5 (2018) 34.

[8] M. Corti, A. Zingaro, L. Dede, A.M. Quarteroni, Impact of atrial fibrillation on left atrium haemodynamics: a computational fluid dynamics study, Comput. Biol. Med. 150 (2022) 106143.

[9] M. Garcia-Villalba, L. Rossini, A. Gonzalo, D. Vigneault, P. Martinez-Legazpi, E. Duran, et al., Demonstration of patient-specific simulations to assess left atrial appendage Thrombogenesis risk, Front. Physiol. 12 (2021) 596596.

[10] A. Masci, M. Alessandrini, D. Forti, F. Menghini, L. Dede, C. Tomasi, et al., A Proof of Concept for computational fluid dynamic analysis of the left atrium in atrial fibrillation on a patient-specific Basis, J. Biomech. Eng. 142 (1) (2020).

[11] X. Morales Ferez, J. Mill, K.A. Juhl, C. Acebes, X. Iriart, B. Legghe, et al., Deep Learning Framework for real-time Estimation of in-silico thrombotic risk indices in the left atrial appendage, Front. Physiol. 12 (2021) 694945.

[12] S. Sanatkhani, S. Nedios, P.G. Menon, A. Bollmann, G. Hindricks, S.G. Shroff, Subject-specific calculation of left atrial appendage blood-Borne particle residence time distribution in atrial fibrillation, Front. Physiol. 12 (2021) 633135.

[13] S. Sanatkhani, S. Nedios, P.G. Menon, S.F. Saba, S.K. Jain, W.J. Federspiel, et al., Subject-specific factors affecting particle residence time distribution of left atrial appendage in atrial fibrillation: a computational model-based study, Front Cardiovasc Med 10 (2023) 1070498.

[14] L. Wang, Z. Wang, R. Fang, Z.Y. Li, Evaluation of stroke risk in patients with atrial fibrillation using morphological and hemodynamic characteristics, Front Cardiovasc Med 9 (2022) 842364.

[15] J. Duenas-Pamplona, J.G. Garcia, J. Sierra-Pallares, C. Ferrera, R. Agujetas, J.R. Lopez-Minguez, A comprehensive comparison of various patient-specific CFD models of the left atrium for atrial fibrillation patients, Comput. Biol. Med. 133 (2021) 104423.

[16] D. Jia, B. Jeon, H.B. Park, H.J. Chang, L.T. Zhang, Image-based flow simulations of Pre- and post-left atrial appendage closure in the left atrium, Cardiovasc Eng Technol 10 (2) (2019) 225–241.

[17] R. Koizumi, K. Funamoto, T. Hayase, M. Kanke, Y. Shibata, Y. Shiraishi, et al., Numerical analysis of hemodynamic changes in the left atrium due to atrial fibrillation, J. Biomech. 48 (3) (2015) 472–478.

[18] D. Vella, A. Monteleone, G. Musotto, G.M. Bosi, G. Burriesci, Effect of the alterations in Contractility and morphology produced by atrial fibrillation on the thrombosis potential of the left atrial appendage, Front. Bioeng. Biotechnol. 9 (2021) 586041.

[19] T. Chen, G. Liu, Y. Mu, W.H. Xu, Y.T. Guo, J. Guo, et al., Application of cardiac computed tomographic imaging and fluoroscopy fusion for guiding left atrial appendage occlusion, Int. J. Cardiol. 331 (2021) 289–295.

[20] Y. Wang, Y.H. Qiao, Y.K. Mao, C.Y. Jiang, J.R. Fan, K. Luo, Numerical prediction of thrombosis risk in left atrium under atrial fibrillation, Math. Biosci. Eng. 17 (3) (2020) 2348–2360.

[21] L. Alinezhad, F. Ghalichi, M. Ahmadlouydarab, M. Chenaghlou, Left atrial appendage shape impacts on the left atrial flow hemodynamics: a numerical hypothesis generating study on two cases, Comput Methods Programs Biomed 213 (2022) 106506.

[22] N. D'Alessandro, M. Falanga, A. Masci, S. Severi, C. Corsi, Preliminary findings on left atrial appendage occlusion simulations applying different endocardial devices, Front Cardiovasc Med 10 (2023) 1067964.

[23] N. Paliwal, R.L. Ali, M. Salvador, R. O'Hara, R. Yu, U.A. Daimee, et al., Presence of left atrial Fibrosis may Contribute to aberrant hemodynamics and increased risk of stroke in atrial fibrillation patients, Front. Physiol. 12 (2021) 657452.

[24] J. Yang, C. Song, H. Ding, M. Chen, J. Sun, X. Liu, Numerical study of the risk of thrombosis in the left atrial appendage of chicken wing shape in atrial fibrillation, Front Cardiovasc Med 9 (2022) 985674.

[25] C. Menichini, X.Y. Xu, Mathematical modeling of thrombus formation in idealized models of aortic dissection: initial findings and potential applications, J. Math. Biol. 73 (5) (2016) 1205–1226.

[26] P. Di Achille, G. Tellides, C.A. Figueroa, J.D. Humphrey, A haemodynamic predictor of intraluminal thrombus formation in abdominal aortic aneurysms, Proc. R. Soc. A 470 (2172) (2014) 20140163.

[27] J. Yang, Z. Bai, C. Song, H. Ding, M. Chen, J. Sun, et al., Research on the Internal flow Field of left atrial appendage and stroke risk Assessment with different blood models, Bioengineering (Basel) 10 (8) (2023).

[28] Z. Zhang, J. Zhu, M. Wu, M. Neidlin, W.T. Wu, P. Wu, Computational modeling of hemodynamics and risk of thrombosis in the left atrial appendage using patient-specific blood viscosity and boundary conditions at the mitral valve, Biomech. Model. Mechanobiol. 22 (4) (2023) 1447–1457.

[29] L. Marroquin, G. Tirado-Conte, R. Pracon, W. Streb, H. Gutierrez, G. Boccuzzi, et al., Management and outcomes of patients with left atrial appendage thrombus prior to percutaneous closure, Heart 108 (14) (2022) 1098–1106.